

A Bayesian framework for local calibration of expensive computational models through non-isometric matching

BABAK FARMANESH, ARASH POURHABIB, BALABHASKAR BALASUNDARAM, AUSTIN
BUCHANAN*

Abstract

We study statistical calibration, i.e., adjusting features of a computational model that are not observable or controllable in its associated physical system. We focus on local, or functional, calibration, which arises in many manufacturing processes where the unobservable features, called calibration variables, are a function of the input variables. A major challenge in many applications is that computational models are expensive and can only be evaluated a limited number of times. Furthermore, without making strong assumptions, the calibration variables are not identifiable. We propose Bayesian non-isometric matching calibration (BNMC) that allows calibration of expensive computational models with only a limited number of samples taken from a computational model and its associated physical system. BNMC replaces the computational model with a dynamic Gaussian Process (GP) whose parameters are trained in the calibration procedure. To resolve the identifiability issue, we present the calibration problem from a geometric perspective of non-isometric curve to surface matching, which enables us to take advantage of combinatorial optimization techniques to extract necessary information for constructing prior distributions. Our numerical experiments demonstrate that in terms of prediction accuracy BNMC outperforms, or is comparable to, other existing calibration frameworks.

Keywords: Local calibration, Gaussian Processes, Generalized minimum spanning tree.

*School of Industrial Engineering and Management, Oklahoma State University, {babak.farmanesh, arash.pourhabib, baski, buchanan}@okstate.edu

1 Introduction

Experimenting on computer models to understand physical systems has become a popular practice ever since computers became advanced enough to handle complex mathematical models and intense computational procedures (Fang et al., 2005, Santner et al., 2013). This popularity is mainly because a computational model can obtain outputs of an experiment in a relatively more cost-effective and timely manner compared to conducting actual experiments in a laboratory. However, one challenge in utilizing computational models is their “adjustment.” In fact, computational models usually incorporate features that cannot be observed or measured in physical systems, but must be correctly specified so that the computational model can accurately resemble the physical system (Kennedy and O’Hagan, 2001). We refer to these unobservable/unmeasurable features as *calibration variables*, and to the adjustment of their values as the *calibration procedure*. We call the input features which are common between the computational models and the physical systems as *control variables*.

For example, in the fabrication of poly-vinyl alcohol (PVA) treated buckypaper, we are interested in understanding the relationship between the response value, which is the tensile strength, and the control variable, which is the PVA amount (Pourhabib et al., 2015). Here, the calibration variable is the percentage of PVA absorbed, which cannot be measured in the physical system, but is required in the computational model.

Past studies on the calibration problem generally assumed unique values for calibration variables, an approach referred to as *global calibration*, and used different statistical approaches to estimate these values. For instance, Kennedy and O’Hagan (2001), Craig et al. (2001), Reese et al. (2004), Higdon et al. (2004, 2008), Williams et al. (2006), Bayarri et al. (2007), and Goldstein and Rougier (2009) devised various Bayesian models, whereas Loepky et al. (2006) and Pratola et al. (2013) used Maximum Likelihood estimation, and Joseph and Melkote (2009) and Han et al. (2009) developed mixed models by combining frequentist and Bayesian methodologies. More recently Tuo and Wu (2015, 2016) developed models based on L_2 distance projection to estimate the true values of the global calibration variables.

In contrast, few studies assume that the values of the calibration variables *depend on the control variables*, which we refer to as *local calibration*. Pourhabib et al. (2015) showed that, for the bucky-

paper fabrication problem, an approach that considers a parametric functional relationship between the amount of PVA and the percentage absorbed can outperform the global calibration approach of Kennedy and O’Hagan (2001). Similarly, Xiong et al. (2009) used a simple linear relationship to improve the calibration accuracy in a benchmark thermal challenge problem. Local calibration approaches that are more general use non-parametric methods to build functional relationships between the calibration variables and the control variables. These non-parametric functional relationships have been constructed using Reproducing Kernel Hilbert Spaces (Schölkopf et al., 2001) and Gaussian Processes (Rasmussen, 2004) by various authors (Pourhabib et al., 2018, Plumlee et al., 2016, Brown and Atamturktur, 2018).

All the aforementioned studies in local calibration and most studies in global calibration require computational models that are “cheaply executable.” This assumption is required since computational models need to be evaluated thousands of times either to draw samples from a posterior distribution in Bayesian approaches, or to numerically minimize a loss function in other approaches. If the computational model is “expensive,” one can obtain a small number of observations from the computational model, then fit a surrogate function based on these random samples, and in the final step replace the computational model in the calibration procedure with this new surrogate model. However, as Section 6 shows this poses a challenge because “static” replacement may result in a poor retrieval of the calibration variables.

Another challenge is the identifiability issue: it is difficult to solve the calibration problem in higher dimensional spaces without making further assumptions on the solution space (Pourhabib et al., 2018). Furthermore, a good prediction performance for the response values does not necessarily imply that a method has accurately captured the functional relationship between the calibration and control variables (Ezzat et al., 2018). This is a significant drawback since, in many applications, understanding the functional relationship between the calibration and control variables is as important as predicting the response values of the system under study.

In this paper, we develop a new framework for the local calibration of expensive computational models. Unlike conventional surrogate modeling, which replaces the computational model with a static, approximated surface, we employ a “dynamic” Gaussian Process (GP) over the computational model. Our GP is dynamic in the sense that the hyper-parameters of the GP’s covariance function are trained during the calibration procedure. We simultaneously construct posterior dis-

tributions for the hyper-parameters of the GP’s covariance function and the calibration variables associated with each of the physical control vectors. In other words, we allow the GP to tune its hyper-parameters in addition to the calibration variables such that the computational model responses become as close as possible to the physical responses.

To tackle the unidentifiability issue in higher-dimensional spaces, we use informative prior distributions. We take advantage of an alternative *geometric interpretation* of calibration, which is non-isometric matching of a curve to a surface. We explain this in the case of a single control variable and a single calibration variable. From a geometric perspective, all possible values for the control variable and the physical response constitute a plane curve in the control-response space (see Figure 1a). In contrast, in the computational model, we can specify the values of both the control and the calibration variables. Consequently, all possible values of the control and calibration variables and the values of the response of the computational model together form a surface. The plane physical curve we observe in the control-response space is a projection of a space curve in the three-dimensional control-calibration-response space.

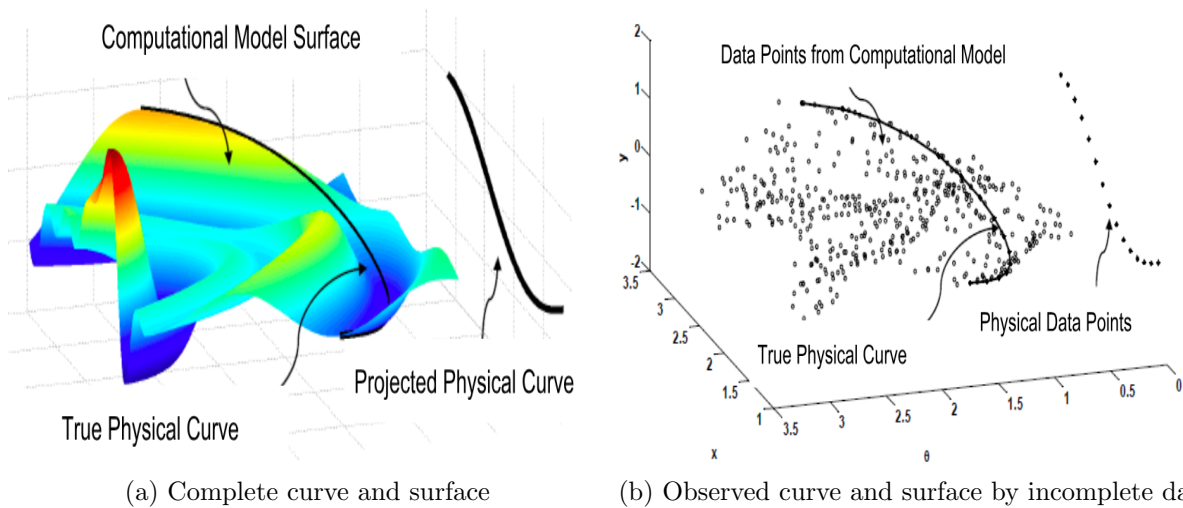


Figure 1: Non-isometric curve to surface matching perspective of local calibration: The left plot shows the complete surface and curve. In practice, we observe a scatter of data points sampled from the complete curve and surface, which is depicted in the right plot.

The geometric interpretation is due to the nature of the calibration variable in a physical process: for each value of the control variable there exists an (unknown) value for the calibration variable, and these two features determine a single response. Since we do not observe the actual value of the

calibration variable in the physical process, we only see a projected curve in the control-response space. Hence, calibration aims to recover the true physical curve, or in other words, determine a non-isometric match of a curve to a surface.

The remainder of this paper is organized as follows. Section 2 explains our Bayesian model for handling expensive computational models. Section 3 formally describes how the calibration problem can be interpreted as a non-isometric curve to surface matching problem. The same section shows how we can utilize this geometric perspective to construct informative prior distributions for our Bayesian model using a graph-theoretic approach. Section 4 generalizes the idea of non-isometric curve to surface matching to higher dimensions and introduces integer programming techniques to tackle the problem. Section 5 uses the approach presented in Sections 3 and 4 to construct informative prior distributions for our Bayesian model and calculates posterior distributions. Section 6 presents our experimental results and compares them with those of previous approaches. Section 7 concludes the paper and presents paths for future research.

2 General Setting: A Bayesian model for calibration

Consider a physical system that operates according to a set of (possibly unknown) physical laws. In this system, there is a functional relationship between a group of features and the response (output). We call those features of the system that can be measured and specified as inputs of the physical system as *control variables*, and denote the vector of these variables by $\mathbf{x} \in \mathbb{R}^{d_x}$. We assume that we obtain data for the physical system by conducting *physical experiments*: once the control variables are set (either observed or specified) in the physical system, the physical process \mathcal{F}^p generates a real-valued response y^p that is

$$y^p = \mathcal{F}^p(\mathbf{x}).$$

Although the response is a function of *all* features of the physical system, we write y^p explicitly as a function of \mathbf{x} as the rest of the features are hard to measure or control, and hence we have no control over them in the physical system. We call such features, *calibration variables*, and categorize them into the following two groups: (i) *global calibration variables*, which have unique values regardless of

the values of the control variables, and (ii) *local calibration variables*, which are functions of control variables.

We denote the vector of global calibration variables by $\boldsymbol{\psi} \in \mathbb{R}^{d^\psi}$ and the vector of local calibration variables by $\boldsymbol{\theta} \in \mathbb{R}^{d^\theta}$. We also denote the function that maps \mathbf{x} to the k^{th} element of $\boldsymbol{\theta}$, i.e., θ_k , by \mathcal{F}_k^θ and the vector of all these functions by $\mathcal{F}^\theta = [\mathcal{F}_1^\theta, \dots, \mathcal{F}_{d^\theta}^\theta]^\top$. With a slight abuse of notation, we denote the vector map from \mathbf{x} to $\boldsymbol{\theta}$ using the vector of functions \mathcal{F}^θ as $\boldsymbol{\theta} = \mathcal{F}^\theta(\mathbf{x})$. Finally, given a positive integer n , we let $[n] := \{1, \dots, n\}$.

Suppose we have a computational model constructed according to the laws governing the physical system. Similar to the physical system, the response of our computational model is determined by the interactions between the control and the calibration variables. However, in a computational model we can set the values of all \mathbf{x} , $\boldsymbol{\theta}$, and $\boldsymbol{\psi}$ arbitrarily within their respective domains. That is because, unlike physical experiments, there are no constraints on measuring or specifying control or calibration variables in a computer model. If we denote the computational process as \mathcal{F}^s , then the response of the computational model can be written as

$$y^s = \mathcal{F}^s(\mathbf{x}, \boldsymbol{\psi}, \boldsymbol{\theta}). \quad (1)$$

By a *computer experiment* we refer to obtaining a value for y^s for a combination of \mathbf{x} , $\boldsymbol{\psi}$, and $\boldsymbol{\theta}$ in the computational model.

The goal of *calibration* is to adjust the variables $\boldsymbol{\psi}$ and $\boldsymbol{\theta}$ such that the computational model represents the physical system in the sense that the computational model can predict the physical response at any input location \mathbf{x}^* .

Mathematically, calibration can be viewed as the estimation of vectors \mathcal{F}^θ and $\boldsymbol{\psi}$ such that, for any given \mathbf{x}^* , the function $\mathcal{F}^s : \mathbb{R}^{d^x} \times \mathbb{R}^{d^\psi} \times \mathbb{R}^{d^\theta} \rightarrow \mathbb{R}$ generates a response close to y^{p^*} up to an error ϵ^* , i.e.,

$$y^{p^*} = \mathcal{F}^s(\mathbf{x}^*, \tilde{\boldsymbol{\psi}}, \tilde{\mathcal{F}}^\theta(\mathbf{x}^*)) + \epsilon^*, \quad (2)$$

where $\tilde{\boldsymbol{\psi}}$ and $\tilde{\mathcal{F}}^\theta$ are estimations of $\boldsymbol{\psi}$ and \mathcal{F}^θ , and the error ϵ^* exists due to assumptions and simplifications made in the computational model and also due to the estimation of the calibration

variables.

To estimate $\tilde{\psi}$ and $\tilde{\mathcal{F}}^\theta$ in (2) we initially obtain m responses from \mathcal{F}^p at a set of physical system inputs $\{\mathbf{x}_1^p, \dots, \mathbf{x}_m^p\}$ to create a dataset P corresponding to that physical system,

$$P := \left\{ p_i = (\mathbf{x}_i^p, y_i^p) \mid \mathbf{x}_i^p \in \mathbb{R}^{d^x}, y_i^p \in \mathbb{R}, i \in [m] \right\}.$$

We also create the counterpart of P in the computational model, i.e., the computational dataset as

$$S := \left\{ s_j = (\mathbf{x}_j^s, \boldsymbol{\psi}_j^s, \boldsymbol{\theta}_j^s, y_j^s) \mid \mathbf{x}_j^s \in \mathbb{R}^{d^x}, \boldsymbol{\psi}_j^s \in \mathbb{R}^{d^\psi}, \boldsymbol{\theta}_j^s \in \mathbb{R}^{d^\theta}, j \in [n] \right\},$$

based on a set of computational model inputs $\{(\mathbf{x}_1^s, \boldsymbol{\psi}_1^s, \boldsymbol{\theta}_1^s), \dots, (\mathbf{x}_n^s, \boldsymbol{\psi}_n^s, \boldsymbol{\theta}_n^s)\}$.

Denoting by $\boldsymbol{\theta}_i^p = \tilde{\mathcal{F}}^\theta(\mathbf{x}_i^p)$ and $\boldsymbol{\psi}^p$ as the estimated values of the calibration variables and assuming that errors are i.i.d. standard normal gives:

$$y_i^p = \mathcal{F}^s(\mathbf{x}_i^p, \boldsymbol{\psi}^p, \boldsymbol{\theta}_i^p) + \epsilon_i^p, \text{ where } \epsilon_i^p \sim \mathcal{N}(0, \sigma^2), \quad \forall i \in [m]. \quad (3)$$

Remark 1. If we remove the local calibration variable $\boldsymbol{\theta}_i^p$ from equation (3), we get a simplified version of the global calibration model proposed in (Kennedy and O’Hagan, 2001). In fact, Kennedy and O’Hagan (2001) assume $y_i^p = \mathcal{F}^s(\mathbf{x}_i^p, \boldsymbol{\psi}^p) + \delta(\mathbf{x}_i^p) + \epsilon_i^p$, where $\delta(\cdot)$ is a GP independent from \mathcal{F}^s , which characterizes all the discrepancy between the computational model and the physical system due to assumptions made in building the computational model. However, because we use a dynamic GP to minimize the discrepancy, we choose to use ϵ_i^p to represent not only the measurement error in the physical system but also the discrepancy between the computational model and the physical system. The reader can refer to the discussion by Tuo and Wu (2016) for a frequentist interpretation of the model proposed by Kennedy and O’Hagan (2001).

Note that applying Bayesian statistics to construct posterior distributions for parameters of model (3), i.e., $\boldsymbol{\psi}^p, \sigma^2$ and $\boldsymbol{\theta}_i^p$ for all $i \in [m]$, requires a large number of evaluations of \mathcal{F}^s , which is not practical for expensive computational models. Therefore, we assume \mathcal{F}^s is a Gaussian Process (Rasmussen, 2004), i.e., $\mathcal{F}^s \sim \mathcal{GP}(0, \mathcal{K}(\cdot, \cdot))$, where $\mathcal{K}(\cdot, \cdot)$ is a covariance function. Here

we use the squared exponential kernel function as the choice of the covariance function,

$$\mathcal{K}(\mathbf{z}, \mathbf{z}') = \gamma \exp(-(\mathbf{z} - \mathbf{z}')^\top \mathbf{L}(\mathbf{z} - \mathbf{z}')), \quad (4)$$

where γ is the magnitude parameter and \mathbf{L} is a diagonal matrix of the length-scale parameters. We denote the vector of the diagonal elements of \mathbf{L} by $\boldsymbol{\ell}$ with length equal to the length of the input vectors \mathbf{z} and \mathbf{z}' .

Subsequently, we can obtain the likelihood of model (3) by the GP distribution defined on \mathcal{F}^s as a multivariate normal distribution,

$$\mathbf{y}^p \mid \mathbf{X}^p, \boldsymbol{\Theta}^p, \boldsymbol{\psi}^p, \boldsymbol{\ell}, \gamma, \sigma^2 \sim \mathcal{N}(0, \boldsymbol{\Sigma} + \sigma^2 \mathbf{I}_m), \quad (5)$$

where $\mathbf{y}^p = [y_1^p, \dots, y_m^p]^\top$ is the vector of physical responses, $\mathbf{X}^p = [\mathbf{x}_1^p, \dots, \mathbf{x}_m^p]^\top$ and $\boldsymbol{\Theta}^p = [\boldsymbol{\theta}_1^p, \dots, \boldsymbol{\theta}_m^p]^\top$ are matrices of size $m \times d^x$ and $m \times d^\theta$ respectively, and $\boldsymbol{\Sigma}$ is the $m \times m$ covariance matrix whose elements are calculated by covariance function (4) with $[\mathbf{x}_i^p, \boldsymbol{\theta}_i^p, \boldsymbol{\psi}^p]^\top$ as input vectors with length $(d^x + d^\theta + d^\psi)$.

Remark 2. Although in the process of deriving likelihood (5), we consider $\boldsymbol{\psi}^p$ and the columns of $\boldsymbol{\Theta}^p$ as the input variables of model (3), we do not know the values of these input variables, and we intend to estimate them. Therefore, in order to distinguish the calibration variables $\boldsymbol{\psi}$ and $\boldsymbol{\theta}$, in (1) from the parameters in model (3), we refer to $\boldsymbol{\Theta}^p$ and $\boldsymbol{\psi}^p$ as calibration parameters.

We can estimate the parameters of model (3), which are the calibration parameters, the parameters of covariance function (4), and the variance of error, simultaneously using Bayesian statistics with the posterior distribution,

$$\pi(\boldsymbol{\Theta}^p, \boldsymbol{\psi}^p, \boldsymbol{\ell}, \gamma, \sigma^2, \mid \mathbf{y}^p, \mathbf{X}^p) \propto \pi(\mathbf{y}^p \mid \mathbf{X}^p, \boldsymbol{\Theta}^p, \boldsymbol{\psi}^p, \boldsymbol{\ell}, \gamma, \sigma^2) \pi(\boldsymbol{\Theta}^p) \pi(\boldsymbol{\psi}^p) \pi(\boldsymbol{\ell}) \pi(\gamma) \pi(\sigma^2). \quad (6)$$

The Bayesian model (6) would be completed by specifying prior distributions for the parameters, i.e., $\pi(\boldsymbol{\Theta}^p)$, $\pi(\boldsymbol{\psi}^p)$, $\pi(\boldsymbol{\ell})$, $\pi(\gamma)$, and $\pi(\sigma^2)$. However, our model suffers from unidentifiability in the absence of weak or uninformative priors due to the high-dimensionality of the parameter space. Therefore, in Section 5 we explain our approach to constructing informative priors for $\boldsymbol{\Theta}^p$ and $\boldsymbol{\psi}^p$ by viewing calibration as a non-isometric curve to surface matching problem.

Note that one might misinterpret the replacement of \mathcal{F}^s by $\mathcal{GP}(0, \mathcal{K}(\cdot, \cdot))$ as a surrogate modeling approach used in the literature, wherein the computational model is replaced by a fixed surrogate surface, which is in turn trained based on a set of limited samples drawn from the computational model prior to any calibration procedure. In contrast, our approach is fundamentally different from surrogate modeling, since in our model, building and training the GP is a part of the calibration process.

3 Calibration as non-isometric matching: A special case

This section explains how the calibration problem can be viewed as a non-isometric curve to surface matching problem for the special case where $\mathbf{x} \in \mathbb{R}$, $\boldsymbol{\theta} \in \mathbb{R}$, and $\boldsymbol{\psi} \in \emptyset$, which means both control and calibration variables are one-dimensional and no global calibration variable exists. From a geometric perspective, all the possible values for \mathbf{x} and $\mathcal{F}^p(\mathbf{x})$ constitute the curve $(\mathbf{x}, \mathcal{F}^p(\mathbf{x}))$ in a two-dimensional space. In the computational model, however, we can specify the values of both \mathbf{x} and $\boldsymbol{\theta}$. Consequently, all the possible values of \mathbf{x} , $\boldsymbol{\theta}$, and $\mathcal{F}^s(\mathbf{x}, \boldsymbol{\theta})$ together form a surface $(\mathbf{x}, \boldsymbol{\theta}, \mathcal{F}^s(\mathbf{x}, \boldsymbol{\theta}))$ in a three-dimensional space. As we noted in Section 1, the true physical curve lies on the three-dimensional computational model surface, i.e., $(\mathbf{x}, \mathcal{F}^\theta(\mathbf{x}), \mathcal{F}^p(\mathbf{x}))$. However, since we do not observe the actual values of the calibration variables in the physical process, we only see a projected curve in $\mathbf{x} - y$ space (see Figure (1a)). Hence, the calibration problem is to recover the true physical curve, or, in other words, determine a non-isometric match of a curve to a surface.

The non-isometry is due to the fact that the curve $(\mathbf{x}, \mathcal{F}^\theta(\mathbf{x}), \mathcal{F}^p(\mathbf{x}))$ on the three-dimensional $\mathbf{x} - \boldsymbol{\theta} - y$ space has a different length than the projected curve $(\mathbf{x}, 0, \mathcal{F}^p(\mathbf{x}))$ on a two-dimensional $\mathbf{x} - y$ space. Therefore, this is, in principle, different from isometric matching problems (Gruen and Akca, 2005, Bronstein et al., 2005, Baltsavias et al., 2008).

Furthermore, in practice we only have the finite physical system dataset P along with a finite computational model dataset S , as we do not observe a complete curve or surface, but a scatter of data points from P and S . Ideally, the points from the former lie on the projected curve that we observe, and the points from the latter lie on the computational model surface (see Figure 1b). Hence, what we observe is incomplete data, and we aim to match non-isometrically an incomplete curve to an incomplete surface, which is equivalent to solving the calibration problem.

This geometric perspective that the calibration problem is a non-isometric curve to surface matching problem, and that we are provided with a finite set of data points from the curve and the surface, motivates us to view the problem through a combinatorial lens and model the problem using graph-theoretic approaches. Our graph-based solution to the non-isometric curve to surface matching problem provides us with a set of computational model data points, which carry information about the calibration parameters. We call this set of computational data points *anchor points*. These anchor points will then be used in Section 5 to construct prior distributions for our Bayesian model.

We seek to identify a set of anchor points among the computational data points, which intuitively are “close” to the points on the true physical curve. In other words, the anchor points are positioned such that the true physical curve passes through neighborhoods of those points. To find these anchor points, we desire two properties: (i) the computational model response should be close to the physical response for a given input \mathbf{x} ; and (ii) the calibration parameter values for two consecutive anchor points should be close to each other. The former drives our method to identify the anchor points that have similar responses as that of the physical system, and the latter aims to encourage the smoothness of the physical curve.

Note that we are only interested in identifying these “optimal” anchor points that provide us with information about the true physical curve to be used in our prior distributions, and not the true physical curve itself. However, one could also directly use the selected anchor points to approximate the true physical curve via interpolation. Given our focus on expensive computational models wherein the number of computational model data points is limited, the approximation of the true physical curve may not be accurate. In the next section, we formally define and address the problem of finding anchor points with the desired properties using a graph-theoretic approach for the special case when $\mathbf{x} \in \mathbb{R}$, $\boldsymbol{\theta} \in \mathbb{R}$, and $\boldsymbol{\psi} \in \emptyset$.

3.1 A graph-theoretic approach for finding anchor points

Without loss of generality, we assume that all the data points in the physical system and the computational model datasets are strictly ordered such that $\mathbf{x}_i^p < \mathbf{x}_{i+1}^p$, for all $i \in [m - 1]$, and $\mathbf{x}_j^s < \mathbf{x}_{j+1}^s$, for all $j \in [n - 1]$. Then, we construct an edge-weighted directed graph $G = (V, E)$ where $V := V^0 \cup \{0, n + 1\}$, and the vertices in $V^0 := [n]$ correspond to the computational model

data points in S . We refer to G as the *calibration digraph*.

Recall that, intuitively speaking, the objective in calibration is to minimize the difference between the outputs of the physical system and the corresponding computational model. As such, the first step is to find control variables that are similar in both settings: the physical experiments and the computer experiments. Therefore, we first group the control variables in the computational model based on their distance to the control variables in the physical experiments. We partition V^0 into m clusters C_1, \dots, C_m as follows: Consider any vertex $j \in V^0$ corresponding to $s_j \in S$. Then, j is assigned to a unique cluster C_i for some $i \in [m]$ by

$$j \in C_i \iff i = \min \left\{ \arg \min_{\ell \in [m]} \{ \|\mathbf{x}_\ell^p - \mathbf{x}_j^s\|_2 \} \right\}. \quad (7)$$

Note that, if the inner minimum in (7) is not unique, then the tie is broken by choosing the smallest index, by the outer minimum. As a consequence, each cluster C_i is in 1-to-1 correspondence with the i^{th} physical data point. We can now describe the set of directed edges E as

$$E := \bigcup_{i \in [m-1]} \{(u, v) \mid u \in C_i, v \in C_{i+1}\} \cup \{(0, u) \mid u \in C_1\} \cup \{(u, n+1) \mid u \in C_m\}.$$

This construction is illustrated in Figure 2.

The final critical step is assigning weights w_{uv} to each edge $(u, v) \in E$. Consider two consecutive clusters C_i and C_{i+1} for any $i \in [m]$ and let $u \in C_i$ and $v \in C_{i+1}$. Define w_{uv} as

$$w_{uv} := |y_u^s - y_u^p| + \lambda \|\boldsymbol{\theta}_u^s - \boldsymbol{\theta}_v^s\|_2, \quad (8)$$

where $\lambda > 0$ is a scaling parameter. The weights $w_{0,u}$ for all $u \in C_1$ and $w_{u,n+1}$ for all $u \in C_m$ are identically zero. The edge-weight for any edge between two consecutive clusters i and $i+1$ consists of two parts: the first part $|y_u^s - y_u^p|$ represents the difference between the model response and physical response (to make sure the outputs of the corresponding physical and computer experiments are close); the second part $\|\boldsymbol{\theta}_u^s - \boldsymbol{\theta}_v^s\|_2$ represents the difference between the calibration parameters of i and $i+1$ (to avoid erratic changes for the calibration parameters). On this digraph G , we intend to solve the shortest path problem from origin vertex 0 to destination vertex $n+1$. Every path from 0 to $n+1$ in G has exactly $m+1$ edges by construction. Therefore, the m internal vertices

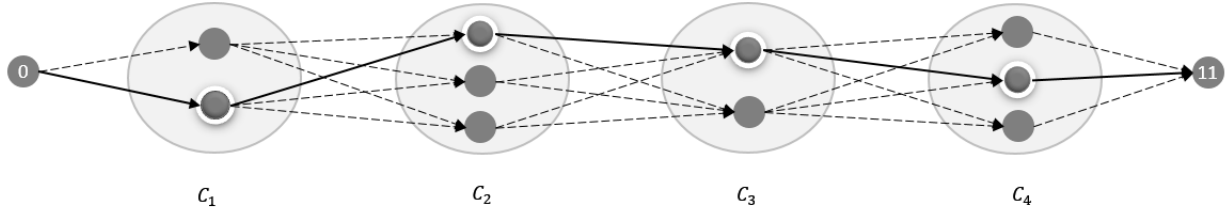


Figure 2: Illustration of the calibration digraph for the case where $m = 4$ and $n = 10$. The vertices represent data points from the computational model and the clusters C_1 through C_m correspond to physical system data points. Vertices denoted by dark circles with a white border represent the anchor points, and the solid arrows identify the edges in the shortest path found.

on the discovered shortest path will serve as the anchor points.

Lemma 1. *Calibration digraph $G = (V, E)$ is acyclic with a topological ordering $\langle 0, 1, \dots, n, n+1 \rangle$.*

Proof. It suffices to show that if $(u, v) \in E$, then $u < v$, which is trivially true when $u = 0$ or $v = n + 1$. For distinct $u, v \in V^0$, note that $u < v \iff \mathbf{x}_u^s < \mathbf{x}_v^s$ as we have assumed the points in S to be strictly ordered. Suppose, $u \in C_i$ and $v \in C_{i+1}$ for some $i \in [m - 1]$. Hence, $\mathbf{x}_i^p < \mathbf{x}_{i+1}^p$, and by (7) we can conclude that the distinct points \mathbf{x}_u^s and \mathbf{x}_v^s satisfy $\mathbf{x}_u^s \leq \frac{1}{2}(\mathbf{x}_i^p + \mathbf{x}_{i+1}^p) \leq \mathbf{x}_v^s$. \square

Since G is a directed acyclic graph, we can solve the shortest path problem using an $\mathcal{O}(|E|)$ algorithm that scans outgoing edges from each vertex in the topological order and updating distance-labels as needed (Bellman, 1958, Lawler, 1976). Suppose $0-v_1-v_2 \dots -v_m-(n+1)$ is the shortest path identified, then those points in S corresponding to $\{v_1, \dots, v_m\}$ serve as the anchor points.

4 Generalization of non-isometric matching to higher dimensions

Section 3 introduced the curve to surface matching interpretation of calibration with $\mathbf{x} \in \mathbb{R}$ and $\boldsymbol{\theta} \in \mathbb{R}$. This special case allowed us to develop a graph-theoretic approach for anchor point selection that admitted a linear-time algorithm. The geometric perspective can be generalized to arbitrary dimensions as a hyper-curve to hyper-surface matching problem. However, in the general setting, there is no straightforward extension of the directed acyclic graph model. Recall that the model hinges on the natural ordering of the computational and the physical data points on the real line, which does not exist in higher dimensions. So, in this section we introduce a different calibration graph model and an associated combinatorial optimization problem to find the anchor points in

an arbitrary dimension. As with the special case, the anchor points will subsequently be used in Section 5 to construct prior distributions for our Bayesian model.

For the general case, we construct a *calibration graph* $G = (V, E)$ that is undirected and edge-weighted, where $V = [n]$ corresponds to the n computational data points. We partition V into m clusters, C_1, \dots, C_m , in correspondence with the m physical data points and assign vertex j to a unique cluster C_i for some $i \in [m]$ by the same rule in (7). The graph G is a complete m -partite graph with partitions C_1, \dots, C_m with the edge set given by $E := \bigcup_{\substack{i, \ell \in [m] \\ i < \ell}} \{\{u, v\} \mid u \in C_i, v \in C_\ell\}$. Figure 3a illustrates this construction.

Finally, before defining the edge-weights, we introduce two required concepts. The *calibration vector* of data point s_j is given by $[\boldsymbol{\theta}_j^{s^\top}, \boldsymbol{\psi}_j^{s^\top}]^\top$. We call two computational data points, $s_u, s_v \in S$, *neighbors* if the Euclidean distance of their control vectors is smaller than a predefined radius r , i.e., $\|\mathbf{x}_u^s - \mathbf{x}_v^s\|_2 < r$.

We assign the weight w_{uv} to the edge $\{u, v\} \in E$, where $u \in C_i$ and $v \in C_\ell$, by

$$w_{uv} := \begin{cases} |y_u^s - y_i^p| + |y_v^s - y_\ell^p| + \lambda \|[\boldsymbol{\theta}_u^{s^\top}, \boldsymbol{\psi}_u^{s^\top}]^\top - [\boldsymbol{\theta}_v^{s^\top}, \boldsymbol{\psi}_v^{s^\top}]^\top\|_2 & \text{if } \|\mathbf{x}_u^s - \mathbf{x}_v^s\|_2 \leq r \\ |y_u^s - y_i^p| + |y_v^s - y_\ell^p| + M \|\mathbf{x}_u^s - \mathbf{x}_v^s\|_2 & \text{if } \|\mathbf{x}_u^s - \mathbf{x}_v^s\|_2 > r, \end{cases} \quad (9)$$

where λ is a scaling parameter and M is a sufficiently large number used to penalize the computational data points that are not close to each other. Note that the weights assigned in (9) extend the idea behind equation (8). Here, the edge-weight between vertices $u \in C_i$ and $v \in C_\ell$, where s_u and s_v are neighbors, consists of two parts, similar to (8): the first part measures the distance between each vertex's response and the physical system response associated with the cluster to which it belongs, i.e., $|y_u^s - y_i^p|$ and $|y_v^s - y_\ell^p|$; the second part measures the distance between the corresponding calibration vectors, i.e., $\|[\boldsymbol{\theta}_u^{s^\top}, \boldsymbol{\psi}_u^{s^\top}]^\top - [\boldsymbol{\theta}_v^{s^\top}, \boldsymbol{\psi}_v^{s^\top}]^\top\|_2$. Let E_1 denote the set of these edges that join all the neighbors. The remainder of the edges, $E_2 = E \setminus E_1$, correspond to edges between computational data points that are not neighbors. We assign relatively large weights to these edges by setting M to a large value. Furthermore, the weight on such edges increases as the distance between the control vectors of the end points increases.

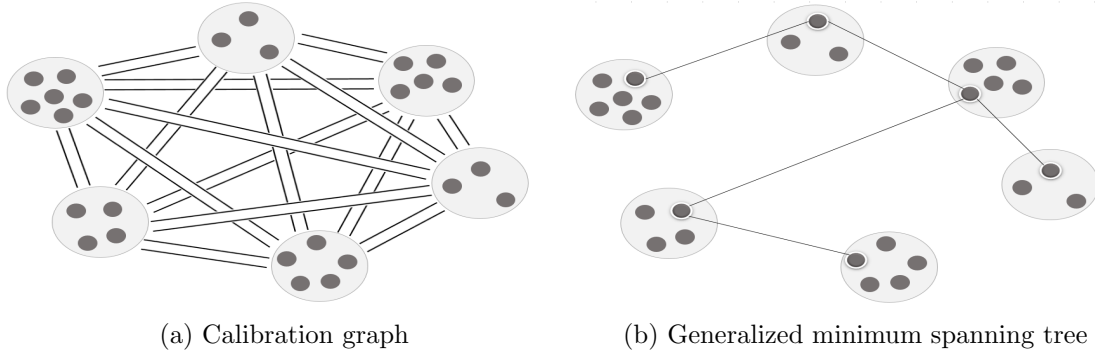


Figure 3: (a) A calibration graph where each black circle represents a vertex and each two parallel lines represent edges between vertices of two clusters. (b) A generalized spanning tree in the calibration graph

To identify the “optimal” anchor vertices on this calibration graph we find a minimum weight tree that contains exactly one vertex from each cluster. In the combinatorial optimization literature, this problem is known as the *generalized minimum spanning tree* (GMST) problem (Myung et al., 1995). By our construction of the edge-weights, a GMST will tend to include edges in E_1 as they are lighter. However, if no GMST exists that only uses edges in E_1 , it will be forced to include edges in E_2 .

4.1 Integer programming approach to GMST problem

The GMST problem was introduced by Myung et al. (1995) who showed that it is NP-hard and does not admit a polynomial-time constant-factor approximation algorithm unless $P=NP$. Various authors (Myung et al., 1995, Feremans et al., 2002, Pop, 2004, Pop et al., 2006) have investigated integer programming (IP) formulations for this problem, in particular, the strength of the associated linear programming (LP) relaxations. This section presents two strong formulations for solving the anchor point selection problem in an arbitrary dimension.

Cutset and subtour elimination formulations for this problem, analogous to those available for the traveling salesman problem and the minimum spanning tree problem (see for instance (Bertsimas and Weismantel, 2005)), were first introduced by Myung et al. (1995) and subsequently advanced by others (Feremans, 2001). These formulations also have directed counterparts, based on the observation that the GMST problem can be viewed as a special case of the *generalized minimum spanning arborescence* (GMSA) problem, wherein we seek an arborescence of minimum

weight in a directed graph that is rooted at some vertex in a specified cluster and contains exactly one vertex per cluster. Here, arborescence refers to a directed graph where there is one, and only one, path between a vertex (called the *root* of the graph) and any other vertex. We can transform the GMST problem to the GMSA problem by replacing each undirected edge $\{i, j\}$ of graph $G = (V, E)$ with anti-parallel arcs (i, j) and (j, i) , also known as the *complete orientation* of G , with each arc assigned the same weight as the undirected edge, and by arbitrarily choosing one of the clusters to contain the root.

In addition to the aforementioned approach with exponentially many constraints, multi-commodity flow based formulations for the problem are also available that use polynomially many constraints and variables (Myung et al., 1995, Feremans et al., 2002, Pop, 2004, Pop et al., 2006). For a detailed review of the IP formulations available for this problem and a comparison of the strength of their LP relaxations, we refer the reader to the analysis by Feremans et al. (2002).

Feremans et al. (2002) showed that a strengthening of the directed counterpart of the subtour elimination formulation, which they call the *directed cluster subpacking* (DCSUB) formulation, is among the strongest in terms of the tightness of the LP relaxation, but uses exponentially many constraints. For the remainder of this discussion, we assume that we have the complete orientation $\overleftrightarrow{G} = (V, A)$ of the calibration graph $G = (V, E)$, where $A := \{a = (u, v), \overleftarrow{a} = (v, u) \mid \{u, v\} \in E\}$. The edge weight of each $\{u, v\} \in E$ is duplicated as arc-weights $w_a = w_{\overleftarrow{a}} := w_{uv}$ for the corresponding arcs $a = (u, v), \overleftarrow{a} = (v, u)$. We require the arborescence to be root at some vertex in C_1 . Recall that the vertex set V is partitioned into clusters C_1, \dots, C_m . In the formulations that follow, $A(Q) := \{(u, v) \in A \mid u, v \in Q\}$ denotes the subset of arcs that have both endpoints in the vertex subset Q . We also use the notations $\delta^+(u)$ and $\delta^-(u)$ to refer to the subsets of arcs that point towards and away from node u , respectively. We use binary decision vectors $q \in \{0, 1\}^{|A|}$ and $b \in \{0, 1\}^{|V|}$ to denote the incidence vectors of the arcs and vertices included in the arborescence,

respectively.

$$\text{(DCSUB)} \quad \min \sum_{a \in A} w_a q_a \tag{10a}$$

$$\text{subject to:} \quad \sum_{v \in C_i} b_v = 1 \quad \forall i \in [m] \tag{10b}$$

$$q_a + q_{\overleftarrow{a}} \leq 1 \quad \forall a, \overleftarrow{a} \in A \tag{10c}$$

$$\sum_{a \in A} q_a = m - 1 \tag{10d}$$

$$\sum_{a \in A(Q)} q_a \leq \sum_{v \in Q} b_v - 1 \quad \forall Q \subset V \text{ such that } Q \supset C_i \text{ for some } i \in [m] \tag{10e}$$

$$\sum_{a \in \delta^-(v)} q_a = b_v \quad \forall v \in V \setminus C_1 \tag{10f}$$

$$b \in \{0, 1\}^{|V|}, q \in \{0, 1\}^{|A|}. \tag{10g}$$

Constraints (10b) enforce that the model chooses exactly one vertex from each cluster, constraints (10d) ensure that exactly $m - 1$ arcs from A are selected, and constraints (10c) ensure that these correspond to $m - 1$ distinct edges in E . Cluster subpacking constraints (10e) prevent solutions that contain cycles and were shown by Feremans et al. (2002) to dominate the more familiar subtour elimination constraints introduced by Myung et al. (1995):

$$\sum_{a \in A(S)} q_a \leq \sum_{v \in S \setminus \{u\}} b_v \quad \forall u \in S \subset V, \quad 2 \leq |S| \leq |V| - 1.$$

Finally, constraints (10f) ensure that every non-root vertex selected by the solution has exactly one incoming edge and every vertex outside C_1 that is not selected will have no incoming arcs; along with the requirement that we choose exactly m vertices and $m - 1$ arcs without creating cycles, this ensures that we obtain an arborescence rooted at some vertex inside C_1 .

Next we present the multi-commodity flow (MCF) formulation for the GMSA problem that avoids using exponentially many constraints, but uses an additional set of variables (Myung et al., 1995). The MCF formulation treats every vertex $v \in C_1$ to have supply b_v for each commodity $i \in \{2, \dots, m\}$ corresponding to the remaining clusters; it treats every $v \in C_i$ to have a demand of b_v for commodity i . Suppose $b_v = 1$ for some $v \in C_i$, then a path must be traced from the root

selected in C_1 to deliver commodity i . We use the additional set of commodity-flow variables f_a^i to denote the amount of commodity $i \in \{2, \dots, m\}$ flowing on arc $a \in A$.

$$\text{(MCF)} \quad \min \sum_{a \in A} q_a w_a \tag{11a}$$

subject to: (10b), (10c), (10d), (10g)

$$\sum_{a \in \delta^+(v)} f_a^i - \sum_{a \in \delta^-(v)} f_a^i = \begin{cases} b_v, & v \in C_1 \\ -b_v, & v \in C_i \\ 0, & v \notin C_1 \cup C_i \end{cases} \quad \forall i \in \{2, \dots, m\} \tag{11b}$$

$$0 \leq f_a^i \leq q_a \quad \forall a \in A, i \in \{2, \dots, m\}. \tag{11c}$$

Constraints (11b) are flow-balance constraints for each commodity, and constraints (11c) prevent flows on the edges that are not selected.

Formulations (10) and (11) are both equally good in terms of the tightness of the LP relaxations as the projection of the LP relaxation of the latter onto the (b, q) -space is the same as the LP relaxation of the former (Feremans et al., 2002). As noted before, MCF is compact while DCSUB has exponentially many cycle elimination constraints. Consequently, a direct monolithic implementation of formulation (10) is impractical even for small scale problems.

Nonetheless, a delayed constraint generation approach could be effective in practice (Buchanan et al., 2015, Moradi and Balasundaram, 2015). This approach starts by relaxing formulation (10) by omitting constraints (10e). During the normal progress of an LP relaxation based branch-and-bound algorithm to solve the relaxed IP, whenever integral solutions are detected, it is necessary to verify if any violated constraint exists among those that were initially excluded and add them to the model. This ensures the overall correctness of the algorithm. An effective implementation of such an algorithm is possible using the “lazy cut” feature of most state-of-the-art commercial IP solvers as long as separation of the violated cycle constraints can be accomplished quickly.

4.2 Comparing GMST and shortest path models for the special case

Before proceeding to discuss our approach to the construction of Bayesian prior distributions and the role that the anchor points play in this approach, we conclude Section 4 by discussing how the

GMST model compares with the shortest path model for the special case.

Suppose that the radius r used in the GMST model is chosen large enough so that even the farthest vertices in two consecutive clusters C_i and C_{i+1} would be considered neighbors, and suppose this is the case for all $i \in [m-1]$. Then, a shortest path found in the special case corresponds to, via the the underlying undirected path, a feasible solution to the GMST model, since that path is also a tree that connects exactly one vertex from each cluster in the underlying graph. Furthermore, the cost of this feasible solution in the GMST model is precisely the length of the shortest path found in the calibration digraph assuming that the same scaling parameter λ is used.

Conversely, the underlying graph of the calibration digraph in Section 3.1 would be obtained in the GMST model if we considered E_2 to include all edges between two non-consecutive clusters and E_1 to include those between consecutive clusters instead of using the radius r to determine which edges belong to E_1 . If we further assume M to be infinitely large, or equivalently deleted from the calibration graph, then we can see that a GMST on this graph that only contained edges from E_1 would correspond precisely to a shortest path in the calibration digraph with the same cost.

The GMST model admits trees (and not just paths) as solutions and does not exclude the edges in E_2 . In the presence of the parameters r and M , these models are incomparable in general. However, while potentially being a more flexible model, the GMST problem is NP-hard in general. Pertinently, the IP approach does not necessarily take into advantage the geometric characteristics of the special case as the shortest path model does. But by doing so, the potentially more restrictive shortest path model is linear-time solvable. This can be helpful if n is significantly large. Despite our focus on calibrating expensive computational models, the computationally favorable shortest path model for the special case makes it a worthwhile alternative to consider when applicable. We also remark here that the shortest path model also does not require the user to select model parameters r and M like the GMST model, while both require λ . Apropos the parameter choice, we offer some empirical guidelines in Section 6.

5 Prior and posterior distributions

This section describes how the information about the true physical curve carried by the anchor points, found by approaches discussed in Sections 3 and 4, can be used to construct our prior

distributions for the calibration parameters. We also expand posterior distribution (6) using the priors specified in this section, and show how we can make predictions at a new control vector \mathbf{x}^* .

Suppose $\boldsymbol{\theta}_i^a$ and $\boldsymbol{\psi}_i^a$ are, respectively, the local and the global calibration vectors of the anchor point associated with the i^{th} physical data point, i.e., the anchor vertex selected from the i^{th} cluster. Define the matrix $\boldsymbol{\Theta}^a := [\boldsymbol{\theta}_1^a, \dots, \boldsymbol{\theta}_m^a]^\top$ of size $m \times d^\theta$ and the mean vector $\boldsymbol{\psi}^a := \frac{1}{m} \sum_{i=1}^m \boldsymbol{\psi}_i^a$ of length d^ψ . Note that for the latter we take the average of the global calibration vectors of the anchor points since we assume that the global calibration parameters are constant regardless of the values of the control vectors.

For each component of $\boldsymbol{\psi}^p$, we consider a univariate normal distribution centered at the corresponding element in $\boldsymbol{\psi}^a$ with an unknown variance as the choice of the prior distribution. Therefore, we construct the prior distribution for $\boldsymbol{\psi}^p$ as

$$\boldsymbol{\psi}^p \mid \boldsymbol{\psi}^a, \boldsymbol{\tau}^2 \sim \mathcal{N}(\boldsymbol{\psi}^a, \text{diag}(\boldsymbol{\tau}^2)), \quad (12)$$

where $\boldsymbol{\tau}^2 = [\tau_1^2, \dots, \tau_{d^\psi}^2]^\top$ is the vector of variances of the normal distribution.

Applying the same procedure for constructing prior distributions for the local calibration parameters increases the dimension of the parameter space, since we need to define md^θ variance parameters, which are nuisance parameters and not of interest to our model. Therefore, in order to shrink the parameter space, we use the fact that the k^{th} column of $\boldsymbol{\Theta}^p$, i.e. $\boldsymbol{\Theta}_k^p$, is actually a realization of the functional relationship \mathcal{F}_k^θ . Therefore, the k^{th} column of $\boldsymbol{\Theta}^a$, i.e., $\boldsymbol{\Theta}_k^a$, is a rough estimator of this realization. On this basis, we use a single variance parameter for all the elements in $\boldsymbol{\Theta}_k^p$, and construct the prior distribution for $\boldsymbol{\Theta}_k^p$ as

$$\boldsymbol{\Theta}_k^p \mid \boldsymbol{\Theta}_k^a, \nu_k^2 \sim \mathcal{N}(\boldsymbol{\Theta}_k^a, \nu_k^2 \mathbf{I}_m), \quad (13)$$

where ν_k^2 is the k^{th} element of the vector of variances $\boldsymbol{\nu}^2$ with length d^θ .

The correctness of the normality assumptions in (12) and (13) is a legitimate concern, because there is no guarantee that the anchor points embrace the true physical curve due to the limited number of observations. However, we only make the normality assumptions in (12) and (13) for constructing the prior distributions, and the Bayesian model will adjust these priors by likelihood (5).

To specify the posterior distribution, we define proper prior distributions for the rest of the parameters. As such, we get:

$$\pi(\Theta^p, \psi^p, \nu^2, \tau^2, \ell, \gamma, \sigma^2 \mid \mathbf{y}^p, \mathbf{X}^p, \Theta^a, \psi^a) \propto \pi(\mathbf{y}^p \mid \mathbf{X}^p, \Theta^p, \psi^p, \ell, \gamma, \sigma^2) \pi(\Theta^p \mid \Theta^a, \nu^2) \pi(\psi^p \mid \psi^a, \tau^2) \pi(\nu^2) \pi(\tau^2) \pi(\ell) \pi(\gamma) \pi(\sigma^2),$$

where,

$$\begin{aligned} \mathbf{y}^p \mid \mathbf{X}^p, \Theta^p, \psi^p, \ell, \gamma, \sigma^2 &\sim \mathcal{N}(0, \Sigma + \sigma^2 \mathbf{I}_m), \\ \Theta_k^p \mid \Theta_k^a, \nu_k^2 &\sim \mathcal{N}(\Theta_k^a, \nu_k^2 \mathbf{I}_m), & \forall k \in [d^\theta], \\ \psi^p \mid \psi^a, \tau^2 &\sim \mathcal{N}(\psi^a, \text{diag}(\tau^2)), \\ \nu_k^2 &\sim \frac{1}{\nu_k^2}, & \forall k \in [d^\theta], \\ \tau_h^2 &\sim \text{Inv-Gamma}(\alpha_\tau, \beta_\tau), & \forall h \in [d^\psi], \\ \ell_j &\sim \text{Log-Gamma}(\alpha_\ell, \beta_\ell), & \forall j \in [d^x + d^\theta + d^\psi], \\ \gamma &\sim \text{Log-Uniform}, \\ \sigma^2 &\sim \text{Log-Uniform}. \end{aligned}$$

For each ν_k^2 we use a flat Jeffreys prior (Jeffreys, 1946), which is an inverse gamma distribution with zero value for both the shape and the scale parameter. For each τ_h^2 we choose a weak inverse gamma distribution, i.e., an inverse gamma with large variance, with $\alpha_\tau = 2.1$ and $\beta_\tau = 10$ as its parameters. Note that both of these prior distributions are conjugate for their associated parameters in the posterior distribution. Moreover, as recommended by Gelman et al. (2014), to improve the identifiability of the model we use the prior distributions on the logarithmic scale for parameters of the GP part of the model. Therefore, for σ^2 and γ we use a flat log-uniform distribution and for each ℓ_j we use a log-gamma distribution with the parameters $\alpha_\ell = \beta_\ell = 2$. Hence, we obtain the

full posterior distribution as

$$\begin{aligned}
& \pi(\boldsymbol{\Theta}^p, \boldsymbol{\psi}^p, \boldsymbol{\nu}^2, \boldsymbol{\tau}^2, \boldsymbol{\ell}, \gamma, \sigma^2 \mid \mathbf{y}^p, \mathbf{X}^p, \boldsymbol{\Theta}^a, \boldsymbol{\psi}^a) \\
& \propto |\boldsymbol{\Sigma} + \sigma \mathbf{I}_m|^{-0.5} \exp \left\{ \frac{-1}{2} \mathbf{y}^p \top (\boldsymbol{\Sigma} + \sigma \mathbf{I}_m)^{-1} \mathbf{y}^p \right\} \\
& \times \prod_k (\nu_k^2)^{-m/2-1} \exp \left\{ \frac{-1}{2\nu_k^2} (\boldsymbol{\Theta}_k^p - \boldsymbol{\Theta}_k^a) \top (\boldsymbol{\Theta}_k^p - \boldsymbol{\Theta}_k^a) \right\} \\
& \times \prod_h (\tau_h^2)^{-1/2-\alpha_\tau-1} \exp \left\{ \frac{-1}{2\tau_h^2} (\psi_h - \psi_h^a)^2 \right\} \exp \left\{ \frac{-\beta_\tau}{\tau_h^2} \right\} \\
& \times \prod_j \frac{1}{\ell_j} \log(\ell_j)^{\alpha_\ell-1} \exp \{-\beta_\ell \log(\ell_j)\} \\
& \times \frac{1}{\gamma} \times \frac{1}{\sigma^2}.
\end{aligned} \tag{14}$$

We use Gibbs sampling (Gelfand et al., 1990) to sequentially sample from the full conditional posterior distributions. Note that the full conditional posterior distributions of all the parameters except ν_k^2 and τ_h^2 , which have inverse gamma distributions, require taking Metropolis-Hastings (Metropolis et al., 1953) steps due to their unknown forms.

In order to make predictions at a new control vector \mathbf{x}^* , first its associated local calibration vector, i.e., $\boldsymbol{\theta}^* = \mathcal{F}^\theta(\mathbf{x}^*)$, should be predicted. We predict the k^{th} element of $\boldsymbol{\theta}^*$, i.e., θ_k^* , by fitting a GP regression to \mathcal{F}_k^θ using the samples drawn from the posterior distribution (14). Let $\boldsymbol{\Theta}^p(t)$ be t^{th} draw from the posterior distribution (14) after some burn-in period, where $t \in [T]$. We note that $\boldsymbol{\Theta}_k^p(t)$ in fact is a vector of estimations of \mathcal{F}_k^θ at the design locations $\{\mathbf{x}_1^p, \dots, \mathbf{x}_m^p\}$, thus we can write $\boldsymbol{\Theta}_k^p(t) = [\mathcal{F}_k^\theta(\mathbf{x}_1), \dots, \mathcal{F}_k^\theta(\mathbf{x}_m)]^\top + [\epsilon_1^\theta, \dots, \epsilon_m^\theta]^\top$, where $[\epsilon_1^\theta, \dots, \epsilon_m^\theta]$ is a vector of the corresponding error terms. Note that the error term appears because $\boldsymbol{\Theta}_k^p(t)$ does not contain exact evaluations of the function \mathcal{F}_k^θ but only estimations.

Assuming $[\epsilon_1^\theta, \dots, \epsilon_m^\theta]^\top \sim \mathcal{N}(0, \sigma_k^\theta \mathbf{I}_m)$ and $\mathcal{F}_k^\theta \sim \mathcal{GP}(0, \mathcal{K}(\cdot, \cdot))$, i.e., \mathcal{F}_k^θ follows a GP distribution with mean zero and covariance function \mathcal{K} , results in a normal distribution for $\boldsymbol{\Theta}_k^p(t)$:

$$\boldsymbol{\Theta}_k^p(t) \sim \mathcal{N}(0, \boldsymbol{\Sigma}_{\mathbf{X}^p \mathbf{X}^p} + \sigma_k^\theta \mathbf{I}_m), \tag{15}$$

where we denote the covariance between columns of matrices \mathbf{Z} and \mathbf{Z}' by $\boldsymbol{\Sigma}_{\mathbf{Z}\mathbf{Z}'}$. We add the variance of error, σ_k^θ , to preserve the smoothness of \mathcal{F}_k^θ ; otherwise, our approach would obtain \mathcal{F}_k^θ

as the interpolation of the elements of $\Theta_k^p(t)$.

By the GP assumption on \mathcal{F}_k^θ , we can obtain the joint distribution of $\Theta_k^p(t)$ and the prediction of θ_k^* for the t^{th} draw, which we denote by $\theta_k^*(t)$, as

$$\begin{bmatrix} \Theta_k^p(t) \\ \theta_k^*(t) \end{bmatrix} \sim \mathcal{N} \left(0, \begin{bmatrix} \Sigma_{\mathbf{X}^p \mathbf{X}^p} + \sigma_k^\theta \mathbf{I}_m & \Sigma_{\mathbf{X}^p \mathbf{X}^*} \\ \Sigma_{\mathbf{X}^* \mathbf{X}^p} & \Sigma_{\mathbf{X}^* \mathbf{X}^*} \end{bmatrix} \right). \quad (16)$$

By conditioning on $\Theta_k^p(t)$ in (16), the point prediction of $\theta_k^*(t)$ is obtained as

$$\theta_k^*(t) = \Sigma_{\mathbf{X}^* \mathbf{X}^p} (\Sigma_{\mathbf{X}^p \mathbf{X}^p} + \sigma_k^\theta \mathbf{I}_m)^{-1} \Theta_k^p(t). \quad (17)$$

Note that for each prediction in (17), the hyper-parameters of the covariance function used in (15) should be tuned, which can be achieved by maximizing the logarithm of likelihood corresponding to (15) (Rasmussen, 2004):

$$\log(\pi(\Theta_k^p(t))) = -\frac{n}{2} \log(2\pi) - \frac{1}{2} \log |\Sigma_{\mathbf{X}^p \mathbf{X}^p} + \sigma_k^\theta \mathbf{I}_m| - \frac{1}{2} \Theta_k^{p\top}(t) (\Sigma_{\mathbf{X}^p \mathbf{X}^p} + \sigma_k^\theta \mathbf{I}_m)^{-1} \Theta_k^p(t).$$

To find point and interval predictions for the new response y^* , we make T predictions based on the T samples we drew from the posterior (14) and the T predictions we made for the vector θ^* using (17). To this end let $\psi^p(t)$, $\ell(t)$, $\gamma(t)$, and $\sigma^2(t)$ be the t^{th} samples from posterior (14), and $\theta^*(t) = [\theta_1^*(t), \dots, \theta_{d_\theta}^*(t)]^\top$ be the prediction of the local calibration vector obtained from (17). Recall from Section 2 that $\mathcal{F}^s \sim \mathcal{GP}(0, \mathcal{K}(\cdot, \cdot))$; therefore, we can use the GP predictive distribution to derive the t^{th} prediction as

$$\begin{aligned} \mathcal{F}^s(\mathbf{x}^*, \theta^*(t), \psi^p(t)) &\sim \mathcal{N} \left(\Sigma_{\mathbf{v}^*(t) \mathbf{v}(t)} (\Sigma_{\mathbf{v}(t) \mathbf{v}(t)} + \sigma^2(t) \mathbf{I}_m)^{-1} \mathbf{y}^p, \right. \\ &\quad \left. \Sigma_{\mathbf{v}^*(t) \mathbf{v}^*(t)} - \Sigma_{\mathbf{v}^*(t) \mathbf{v}(t)} (\Sigma_{\mathbf{v}(t) \mathbf{v}(t)} + \sigma^2(t) \mathbf{I}_m)^{-1} \Sigma_{\mathbf{v}(t) \mathbf{v}^*(t)} \right), \end{aligned} \quad (18)$$

where $\mathbf{v}^*(t) = [\mathbf{x}^{*\top}, \theta^{*\top}(t), \psi^{p\top}(t)]^\top$, $\mathbf{v}(t) = [\mathbf{X}^p, \Theta^p(t), \mathbb{1}_{m \times d_\psi} \text{diag}(\psi^p(t))]^\top$, and the covariance matrices are calculated using the t^{th} sample of the covariance parameters, i.e., $\ell(t)$ and $\gamma(t)$.

Finally, we derive our prediction using distribution (18) as

$$\hat{\mu}^* = \frac{1}{T} \sum_{t=1}^T \left(\Sigma_{\mathbf{v}^*(t)\mathbf{v}(t)} (\Sigma_{\mathbf{v}(t)\mathbf{v}(t)} + \sigma^2(t)\mathbf{I}_m)^{-1} \mathbf{y}^p \right),$$

$$\hat{\sigma}^{*2} = \frac{1}{T^2} \sum_{t=1}^T \left(\Sigma_{\mathbf{v}^*(t)\mathbf{v}^*(t)} - \Sigma_{\mathbf{v}^*(t)\mathbf{v}(t)} (\Sigma_{\mathbf{v}(t)\mathbf{v}(t)} + \sigma^2(t)\mathbf{I}_m)^{-1} \Sigma_{\mathbf{v}(t)\mathbf{v}^*(t)} \right).$$

6 Experimental results

In this section, we evaluate the performance of our methodology by testing it on two synthetic problems and two real problems, and compare the results with competing local calibration methodologies, which are non-parametric functional calibration (NFC) (Pourhabib et al., 2018), parametric functional calibration (PFC) (Pourhabib et al., 2015), and non-parametric Bayesian calibration (NBC) (Brown and Atamturktur, 2018). The aforementioned methodologies require surrogate modeling for handling expensive computational models. When we use GMST to find a set of anchor points, we refer to our approach as BMNC. If DAG is used instead, we call the approach BMNC-DAG.

We use the root mean squared error (RMSE) as the measure of accuracy in prediction of responses and calibration vectors to compare the performance of the competing methodologies;

$$\text{RMSE}_y = \sqrt{\frac{1}{n^*} \sum_{q=1}^{n^*} (\hat{y}_q^* - y_q^*)^2} \quad \text{and} \quad \text{RMSE}_\theta = \sqrt{\frac{1}{n^*} \sum_{q=1}^{n^*} \left\| [\hat{\boldsymbol{\theta}}_q^{*\top}, \hat{\boldsymbol{\psi}}_q^{*\top}]^\top - [\bar{\boldsymbol{\theta}}_q^{*\top}, \bar{\boldsymbol{\psi}}_q^{*\top}]^\top \right\|_2^2},$$

where \hat{y}_q^* , $\hat{\boldsymbol{\theta}}_q^*$, and $\hat{\boldsymbol{\psi}}_q^*$ are the predicted response and calibration parameter values for the q^{th} test control variable.

Both the MCF and DCSUB formulations find anchor points for each dataset in less than two minutes on all the instances in our testbed, which shows that both formulations are fast in terms of computation time. To choose proper values of λ , r , and M for the GMST model we use the following empirical approach. First, in order to have the same scale for the inputs and outputs in S and P , before constructing the calibration graph we standardize (divide by the range of each element) the control set $\{\mathbf{x}_i^p, \mathbf{x}_j^s \mid i \in [m], j \in [n]\}$, the calibration set $\{\boldsymbol{\theta}_j^s, \boldsymbol{\psi}_j^s \mid j \in [n]\}$, and the response set $\{y_j^s, y_i^p \mid i \in [m], j \in [n]\}$. We denote the standardized versions of $\mathbf{x}_i^p, \mathbf{x}_j^s, \boldsymbol{\theta}_j^s, \boldsymbol{\psi}_j^s, y_j^s$,

and y_i^p by $\bar{\mathbf{x}}_i^p, \bar{\mathbf{x}}_j^s, \bar{\boldsymbol{\theta}}_j^s, \bar{\boldsymbol{\psi}}_j^s, \bar{y}_j^s$, and \bar{y}_i^p . Note that this standardization is only for finding the anchor points, and once the anchor points are chosen, we transform the data back to their original scales for Bayesian inference. After standardization, λ has to be less than two, otherwise the closeness of the calibration vectors is weighted as more important than closeness of the responses. We choose λ from $\{0.1, 0.5, 1, 1.5\}$ in our experiments. Moreover, for M to be a sufficiently large number, it should be larger than the sum of all the weights on the arcs that can be potentially in E_1 , that is:

$$M \geq \sum_{j \in [n]} \sum_{k \in [n]} \sum_{i \in [m]} \sum_{\ell \in [m]} |\bar{y}_j^s - \bar{y}_i^p| + |\bar{y}_k^s - \bar{y}_\ell^p| + \lambda \left\| [\bar{\boldsymbol{\theta}}_j^{s^\top}, \bar{\boldsymbol{\psi}}_j^{s^\top}]^\top - [\bar{\boldsymbol{\theta}}_k^{s^\top}, \bar{\boldsymbol{\psi}}_k^{s^\top}]^\top \right\|_2.$$

Finally, to choose a proper value for r , we plot the pairwise Euclidean distances between all $\bar{\mathbf{x}}^p$ vectors. Then, we use the fact that each point on this plot represents an existing distance between the centers of two clusters in the calibration graph. Therefore, an upper bound on a group of smallest distances, which are close together and disjoint from other groups of distances, can be used as a proper value for r .

6.1 Description of the calibration problems

The first synthetic problem that we create is to test if the calibration methodologies can recover the local calibration variable in the absence of any global calibration variable. This synthetic problem has two control variables and one local calibration variable. We define

$$\mathcal{F}^s(\mathbf{x}, \theta) = 0.4(x_1^2 + x_2^2) \sin^2(0.7x_2) \frac{x_1 + x_2}{\theta^2 + 1} \quad \text{and} \quad \mathcal{F}^p(\mathbf{x}) = 0.4(x_1^2 + x_2^2) \sin^2(0.7x_2),$$

which implies $\mathcal{F}^\theta(\mathbf{x}) = (x_1 + x_2 - 1)^{0.5}$. We locate $m = 16$ control vectors, \mathbf{x}^p , uniformly on the square $[0, 3.5] \times [0, 3.5]$. Then for each \mathbf{x}^p , we sample 10 local calibration vectors randomly from the interval $[0, 5]$; therefore, we have a total of $n = 160$ computational data points. Finally, we sample 10 random test control vectors, \mathbf{x}^* , from the same square $[0, 3.5] \times [0, 3.5]$ to form a test dataset.

The second synthetic problem was originally used by Brown and Atamturktur (2018) and has one control, one local calibration, and one global calibration variable. The computational and the

physical models are defined as

$$\mathcal{F}^s(x, \theta, \psi) = \theta + \psi x^2 \quad \text{and} \quad \mathcal{F}^p(x) = 2\sqrt{x} + 2.5x^2;$$

therefore, $\psi = 2.5$ and $\mathcal{F}^\theta(x) = 2\sqrt{x}$. We choose $m = 15$ control vectors for training at locations $\{0, 0.05, 0.10, 0.15, 0.20, 0.25, 0.30, 0.35, 0.40, 0.70, 0.75, 0.80, 0.85, 0.90, 0.95\}$, and use five physical control vectors for testing at locations $\{0.45, 0.50, 0.55, 0.60, 0.65\}$. Following the same procedure as the first synthetic problem, we sample 10 local calibration vectors for each \mathbf{x}^p from the square $[0, 5] \times [0, 5]$; therefore, we have a total of $n = 150$ computational data points.

The first real problem from a spot welding application was originally introduced by Bayarri et al. (2007). This problem has three control variables and one calibration variable. The dataset associated with spot welding contains 12 and 35 data points sampled from the physical experiments and the computation model, respectively. The second real problem studied by Pourhabib et al. (2015) has one control variable and one calibration variable, and the associated dataset contains 11 and 150 data points sampled from the physical experiments and the computation model, respectively. This instance arises from a PVA-treated buckypaper fabrication process.

For the real problems, we partition the sets of physical data points using four-fold cross validation to form training and test datasets. Therefore, for each iteration of cross validation for the spot welding dataset, we have eight physical data points in the training set and four physical data points in the test set. Similarly, for the PVA dataset we have eight to nine physical data points in the training set, and two to three data points in the test set in each iteration of cross validation. We note that the cross validation does not affect the size of the computational datasets, i.e., $n = 35$ for spot welding and $n = 150$ for the PVA dataset.

6.2 Results

For each of the aforementioned problems, we choose the values of λ , r , and M following the empirical approach explained in Section 6 (See Table 1). Table 2 compares the performance of BNMC and BNMC-DAG in terms of RMSE_θ and RMSE_y with the other competing methodologies.

The second and third columns of Table 2 show that for the first synthetic problem BNMC has the same order of accuracy as the other competing methodologies in terms of RMSE_θ , but

outperforms them in terms of RMSE_y .

For the second synthetic problem, we only compare the results of NBC and BNMC, since the codes for NFC and PFC are written only for univariate calibration problems. The fourth and the fifth columns of Table 2 show that BNMC outperforms NBC both in terms of RMSE_y and RMSE_θ . We note that the reported RMSE_y for NBC in (Brown and Atamturktur, 2018) under the cheap computational code assumption is 0.0538, which is a better accuracy compared to that of BNMC; however, here BNMC is superior when NBC uses surrogate modeling.

Since the true values of the calibration parameters are unknown for the real problems, we compare the results only in terms of RMSE_y . The sixth column of Table 2 shows the better performance of BNMC compared to the other competing methodologies. We attribute this better performance to the capability of BNMC in handling expensive computational models with a small number of computational data points.

For the PVA problem, since $\mathbf{x} \in \mathbb{R}$, $\boldsymbol{\theta} \in \mathbb{R}$, and $\boldsymbol{\psi} \in \emptyset$, we can use the DAG model discussed in Section 3.1, as well as GMST, to find a set of anchor points. The last column of Table 2 shows that BNMC, BNMC-DAG, and NBC have the same order of accuracy and perform better than NFC and PFC.

Parameter	1 st synthetic problem	2 nd synthetic problem	PVA	Spot Welding
λ	0.5	0.5	0.5	0.5
r	0.9	0.16	0.5	4
M	10^5	10^5	10^5	10^5

Table 1: The calibration graph parameters for the four problems.

Methodology	1 st synthetic problem		2 nd synthetic problem		PVA	Spot Welding
	RMSE_y	RMSE_θ	RMSE_y	RMSE_θ	RMSE_y	RMSE_y
NFC	0.143	0.202	-	-	0.379	0.683
PFC	0.296	0.390	-	-	0.450	1.115
NBC	0.132	0.627	0.172	0.426	0.281	0.516
BNMC	0.076	0.356	0.063	0.354	0.296	0.409
BNMC-DAG	-	-	-	-	0.288	-

Table 2: RMSE_θ and RMSE_y of different methodologies for the four problems.

Figure 4 shows the 95% confidence interval predictions for the responses and the local calibration parameter for the test datasets of the first and the second synthetic problems. Note that since $\mathbf{x}^p \in \mathbb{R}^2$ for the first synthetic problem, we plot the predicted values against their indices in Figures 4a and 4b, and connect the data points to each other for better visualization.

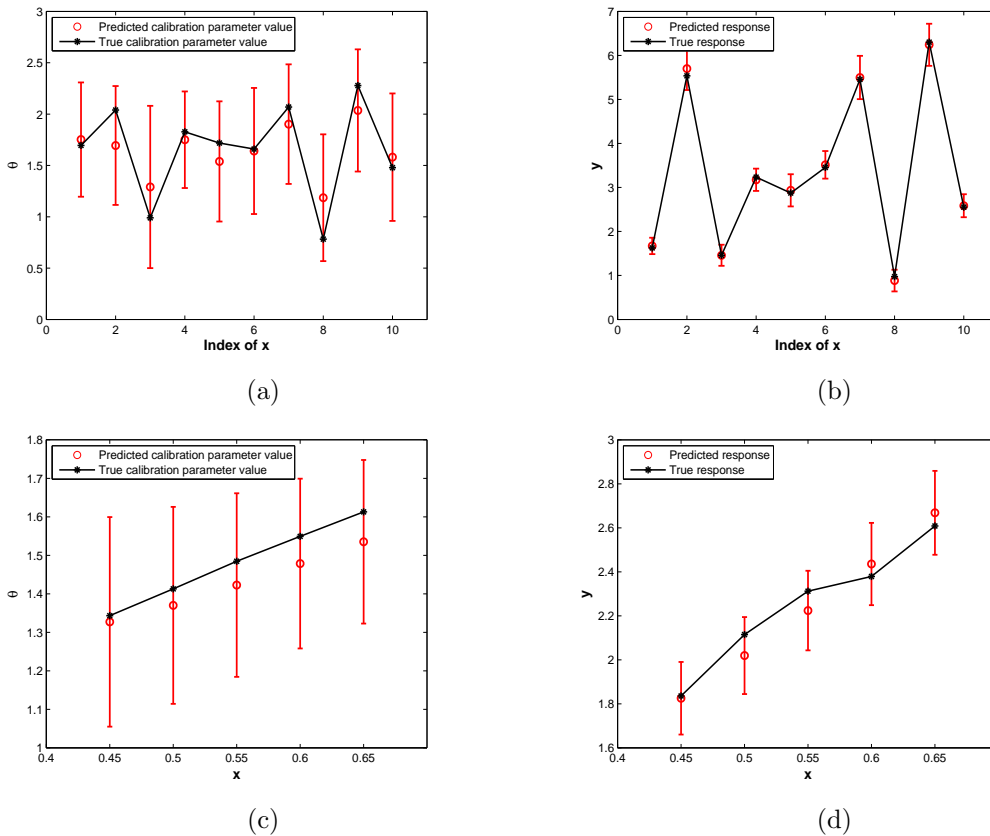


Figure 4: The 95% confidence interval predictions for local calibration parameter values and responses for the test datasets of the first and the second synthetic problems.

As noted in Section 2, due to the limited number of samples we collect from the computational model, we cannot accurately recover \mathcal{F}^θ , but the way we train the hyper-parameters of the GP aims to compensate for this inaccuracy. We can observe this in Figure 4, where the predictions of the response values have better accuracy and tighter confidence intervals compared to those of local calibration parameter values.

For illustration, Figure 5 shows the 95% confidence interval predictions for one of the test datasets created in the cross validation process for each of the spot welding and the PVA problems. Since we do not know the true local calibration parameter values, we cannot provide a similar plot

for the calibration predictions. Similar to Figures 4a and 4b, we plot the predicted values against their indices in Figure 5a for better visualization.

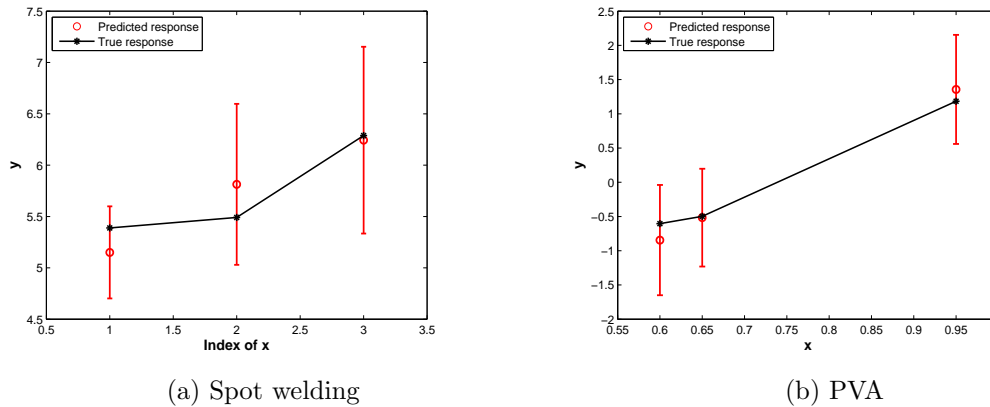


Figure 5: The 95% confidence interval predictions for one of the test datasets created in the cross validation process for each of the spot welding and the PVA problems.

7 Concluding remarks

We proposed a Bayesian non-isometric matching calibration model for expensive computational models. A limited budget to evaluate computational models led to the use of a GP, which was trained *during* the calibration procedure. We used Bayesian statistics to simultaneously train the hyper-parameters of the GP’s covariance function and make inferences on the calibration parameters associated with the physical data points. To construct informative prior distributions for our new approach, we used a geometric interpretation of calibration based on non-isometric curve to surface matching. This point of view enabled us to develop graph-theoretic approaches to address the problem of finding a set of anchor points used in constructing informative prior distributions. For the special case of a single control and calibration variable, we introduced a shortest path model on a directed acyclic calibration graph to tackle the problem of finding anchor points, while for the general case, we introduced the generalized minimum spanning tree model. Our numerical experiments conducted on four benchmark calibration problems showed that our approach outperformed the existing calibration models under the assumption of expensive computational models.

The framework developed in this paper could be extended in several ways. We only considered a single computational data point to construct a prior distribution for each calibration parameter;

however, information of multiple computational data points could be taken into account. An implementation of this idea, of course, requires developing new combinatorial optimization techniques capable of choosing an appropriate number of computational data points. Another interesting research path would be to consider data uncertainty formally in the calibration graph model instead of using a deterministic calibration graph model, and then using Bayesian inference to deal with the uncertainty in the data.

Acknowledgment

Austin Buchanan is supported by the National Science Foundation under Grant No. 1662757. This work was completed utilizing the High Performance Computing Center facilities of Oklahoma State University at Stillwater. The authors also acknowledge Dr. Chuck Zhang from Georgia Institute of Technology for providing the authors with the PVA-treated buckypaper fabrication data.

References

- Baltsavias, E., A. Gruen, H. Eisenbeiss, L. Zhang, and L. Waser (2008). High-quality image matching and automated generation of 3D tree models. *International Journal of Remote Sensing* 29(5), 1243–1259.
- Bayarri, M. J., J. O. Berger, R. Paulo, J. Sacks, J. A. Cafeo, J. Cavendish, C.-H. Lin, and J. Tu (2007). A framework for validation of computer models. *Technometrics* 49(2), 138–154.
- Bellman, R. (1958). On a routing problem. *Quarterly of Applied Mathematics* 16(1), 87–90.
- Bertsimas, D. and R. Weismantel (2005). *Optimization Over Integers*. Belmont, Massachusetts: Dynamic Ideas.
- Bronstein, A. M., M. M. Bronstein, and R. Kimmel (2005). Three-dimensional face recognition. *International Journal of Computer Vision* 64(1), 5–30.
- Brown, D. A. and S. Atamturktur (2018). Nonparametric functional calibration of computer models. *Statistica Sinica* 28, 721–742.
- Buchanan, A., J. S. Sung, S. Butenko, and E. L. Pasilio (2015). An integer programming approach for fault-tolerant connected dominating sets. *INFORMS Journal on Computing* 27(1), 178–188.
- Craig, P. S., M. Goldstein, J. C. Rougier, and A. H. Seheult (2001). Bayesian forecasting for complex systems using computer simulators. *Journal of the American Statistical Association* 96(454), 717–729.
- Ezzat, A. A., A. Pourhabib, and Y. Ding (2018). Sequential design for functional calibration of computer models. *Technometrics* 60(3), 286–296.
- Fang, K.-T., R. Li, and A. Sudjianto (2005). *Design and modeling for computer experiments*. CRC Press.
- Feremans, C. (2001). *Generalized Spanning Trees and Extensions*. Ph. D. thesis, Universite Libré de Bruxelles, Belgium.

- Feremans, C., M. Labbé, and G. Laporte (2002). A comparative analysis of several formulations for the generalized minimum spanning tree problem. *Networks* 39(1), 29–34.
- Gelfand, A. E., S. E. Hills, A. Racine-Poon, and A. F. Smith (1990). Illustration of Bayesian inference in normal data models using Gibbs sampling. *Journal of the American Statistical Association* 85(412), 972–985.
- Gelman, A., J. B. Carlin, H. S. Stern, and D. B. Rubin (2014). *Bayesian Data Analysis*, Volume 2. Chapman & Hall/CRC Boca Raton, FL, USA.
- Goldstein, M. and J. Rougier (2009). Reified Bayesian modelling and inference for physical systems. *Journal of Statistical Planning and Inference* 139(3), 1221–1239.
- Gruen, A. and D. Akca (2005). Least squares 3D surface and curve matching. *ISPRS Journal of Photogrammetry and Remote Sensing* 59(3), 151–174.
- Han, G., T. J. Santner, and J. J. Rawlinson (2009). Simultaneous determination of tuning and calibration parameters for computer experiments. *Technometrics* 51(4), 464–474.
- Higdon, D., J. Gattiker, B. Williams, and M. Rightley (2008). Computer model calibration using high-dimensional output. *Journal of the American Statistical Association* 103(482), 570–583.
- Higdon, D., M. Kennedy, J. C. Cavendish, J. A. Cafo, and R. D. Ryne (2004). Combining field data and computer simulations for calibration and prediction. *SIAM Journal on Scientific Computing* 26(2), 448–466.
- Jeffreys, H. (1946). An invariant form for the prior probability in estimation problems. *Proceedings of the Royal Society of London. Series A, Mathematical and Physical Sciences* 186(1007), 453–461.
- Joseph, V. R. and S. N. Melkote (2009). Statistical adjustments to engineering models. *Journal of Quality Technology* 41(4), 362.
- Kennedy, M. C. and A. O’Hagan (2001). Bayesian calibration of computer models. *Journal of the Royal Statistical Society: Series B (Statistical Methodology)* 63(3), 425–464.
- Lawler, E. (1976). *Combinatorial Optimization: Networks and Matroids*. New York: Holt, Rinehart, and Winston.
- Loeppky, J., D. Bingham, and W. Welch (2006). Computer model calibration or tuning in practice. Technical report, University of British Columbia, Vancouver, BC, CA.
- Metropolis, N., A. W. Rosenbluth, M. N. Rosenbluth, A. H. Teller, and E. Teller (1953). Equation of state calculations by fast computing machines. *The Journal of Chemical Physics* 21(6), 1087–1092.
- Moradi, E. and B. Balasundaram (2015, November). Finding a maximum k -club using the k -clique formulation and canonical hypercube cuts. *Optimization Letters*. See also: Y. Lu, E. Moradi, and B. Balasundaram. Correction to: Finding a maximum k -club using the k -clique formulation and canonical hypercube cuts. *Optimization Letters*, DOI: 10.1007/s11590-018-1273-7, 2018.
- Myung, Y.-S., C.-H. Lee, and D.-W. Tcha (1995). On the generalized minimum spanning tree problem. *Networks* 26(4), 231–241.
- Plumlee, M., V. R. Joseph, and H. Yang (2016). Calibrating functional parameters in the ion channel models of cardiac cells. *Journal of the American Statistical Association* 111(514), 500–509.
- Pop, P. C. (2004). New models of the generalized minimum spanning tree problem. *Journal of Mathematical Modelling and Algorithms* 3(2), 153–166.
- Pop, P. C., W. Kern, and G. Still (2006). A new relaxation method for the generalized minimum spanning tree problem. *European Journal of Operational Research* 170(3), 900–908.

- Pourhabib, A., J. Z. Huang, K. Wang, C. Zhang, B. Wang, and Y. Ding (2015). Modulus prediction of buckypaper based on multi-fidelity analysis involving latent variables. *IIE Transactions* 47(2), 141–152.
- Pourhabib, A., R. Tuo, S. He, J. Z. Huang, and Y. Ding (2018). Local calibration of computer models. Manuscript.
- Pratola, M. T., S. R. Sain, D. Bingham, M. Wiltberger, and E. J. Rigler (2013). Fast sequential computer model calibration of large nonstationary spatial-temporal processes. *Technometrics* 55(2), 232–242.
- Rasmussen, C. E. (2004). Gaussian Processes for Machine Learning. In *Advanced Lectures on Machine Learning*, pp. 63–71. Springer.
- Reese, C. S., A. G. Wilson, M. Hamada, H. F. Martz, and K. J. Ryan (2004). Integrated analysis of computer and physical experiments. *Technometrics* 46(2), 153–164.
- Santner, T. J., B. J. Williams, and W. I. Notz (2013). *The Design and Analysis of Computer Experiments*. Springer Science & Business Media.
- Schölkopf, B., R. Herbrich, and A. J. Smola (2001). A generalized representer theorem. In *International Conference on Computational Learning Theory*, pp. 416–426. Springer.
- Tuo, R. and C. F. J. Wu (2015). Efficient calibration for imperfect computer models. *The Annals of Statistics* 43(6), 2331–2352.
- Tuo, R. and C. F. J. Wu (2016). A theoretical framework for calibration in computer models: Parametrization, estimation and convergence properties. *SIAM/ASA Journal on Uncertainty Quantification* 4(1), 767–795.
- Williams, B., D. Higdon, J. Gattiker, L. Moore, M. McKay, S. Keller-McNulty, et al. (2006). Combining experimental data and computer simulations, with an application to flyer plate experiments. *Bayesian Analysis* 1(4), 765–792.
- Xiong, Y., W. Chen, K.-L. Tsui, and D. W. Apley (2009). A better understanding of model updating strategies in validating engineering models. *Computer Methods in Applied Mechanics and Engineering* 198(15), 1327–1337.